Supporting Information

Coarse-Grained Simulations of Ionic Liquid Materials: From Monomeric Ionic Liquids to Ionic Liquid Crystals and Polymeric Ionic Liquids

Yong-Lei Wang [a,*,†,‡], Bin Li [b,*], Aatto Laaksonen [a,c,d,e]

[a] *Department of Materials and Environmental Chemistry, Arrhenius Laboratory, Stockholm University, SE-10691 Stockholm, Sweden*

[b] *School of Chemical Engineering and Technology, Sun Yat-sen University, Zhuhai 519082, P. R. China*

[c] *State Key Laboratory of Materials-Oriented and Chemical Engineering, Nanjing Tech University, Nanjing 210009, P. R. China*

[d] *Centre of Advanced Research in Bionanoconjugates and Biopolymers, Petru Poni Institute of Macromolecular Chemistry Aleea Grigore Ghica-Voda, 41A, 700487 Iasi, Romania*

[e] *Department of Engineering Sciences and Mathematics, Division of Energy Science, Luleå University of Technology, SE-97187 Luleå, Sweden*

Contents

*These authors contributed equally to this work.

†Author to whom correspondence should be addressed: wangyonl@gmail.com.

‡Present address: Department of Electrochemical Energy Storage, Helmholtz-Zentrum Berlin für Materialien und Energie, Hahn-Meitner-Platz 1, 14109 Berlin, GERMANY.

I. Atomistic models and simulations of $[C_2C_nIM][BF_4]$ ILs

Atomistic models and force field parameters. Atomistic force field (FF) parameters for $[C_2C_nIM][BF_4]$ ILs were developed following a similar procedure that was used in previous works [1–3] based on the AMBER framework. The atom interaction potentials are described in the AMBER FF format:

$$U_{total} = \sum_{bonds} K_r(r-r_0)^2 + \sum_{angles} K_\theta(\theta-\theta_0)^2 + \sum_{torsions} \frac{K_\phi}{2}[1+\cos(n\phi-\gamma)] + \sum_{i<j}\left\{4\epsilon_{ij}[(\frac{\sigma_{ij}}{r_{ij}})^{12}-(\frac{\sigma_{ij}}{r_{ij}})^{6}]+\frac{q_iq_j}{4\pi\epsilon_0\epsilon_r r_{ij}}\right\}. \quad (1)$$

The first three terms represent bonded interactions, *i.e.*, bond stretching, angle bending, and dihedral interactions, and the corresponding potential parameters have their usual meaning [1, 2]. The nonbonded interactions are described in the last term, including van der Waals (vdW, here Lennard-Jones 12-6 form) and Coulombic interactions of atom-centered point charges. The vdW interactions are calculated between atoms in different molecules or atoms in the same molecule that are separated by more than three consecutive bonds. The vdW interaction parameters between different atoms are obtained from the Lorentz-Berthelot combining rule with $\epsilon_{ij}=\sqrt{\epsilon_{ii}\epsilon_{jj}}$ and $\sigma_{ij}=(\sigma_{ii}+\sigma_{jj})/2$. The nonbonded interactions separated by exactly three consecutive bonds (1-4 interactions) are reduced by related scaling factors, which are optimized as 0.50 for vdW interactions and 0.83 for electrostatic interactions [1, 2].

Atomistic simulation methodology. All-atomistic molecular dynamics (AA MD) simulations of $[C_2C_nIM][BF_4]$ ILs with n=2, 4, 8, and 12 were first performed to provide reference thermodynamics, structural, and dynamical quantities to validate the constructed CG model and the derived interaction parameters for CG beads. Each simulation system consists of a varied number of $[C_2C_nIM][BF_4]$ ion pairs with the total number of atoms of approximately 30000. That is, the $[C_2C_2IM][BF_4]$, $[C_2C_4IM][BF_4]$, $[C_2C_8IM][BF_4]$, and $[C_2C_{12}IM][BF_4]$ modelling systems are consisting of 1250, 1000, 715, and 556 ion pairs, respectively. Additional atomistic simulations of $[C_2C_{16}IM][BF_4]$ and $[C_2C_{20}IM][BF_4]$ ILs consisting of 455 and 385 ion pairs, respectively, were performed to estimate liquid densities of these two modelling systems at varied temperatures. Such an atomistic simulation system composition leads to the length of cubic simulation box of approximately 63.2548 and 62.5876 Angstrom for $[C_2C_{16}IM][BF_4]$ and $[C_2C_{20}IM][BF_4]$ ILs, respectively, at room temperature.

Atomistic simulations were performed using the GROMACS package with cubic periodic boundary conditions [4]. The equations of motion were integrated using a classical velocity Verlet leap-frog integration algorithm with a time step of 1.0 fs. A cutoff distance of 1.6 nm was set for short range vdW interactions and real-space electrostatic interactions between atomic partial charges to improve the computatioanl efficiency of atomistic simulations at extended time scales. The particle-mesh Ewald summation method was employed to handle long range electrostatic interactions in reciprocal space with an interpolation order of 5 and a Fourier grid spacing of 0.2 nm. All simulation systems were first energetically minimized using a steepest descent algorithm, and thereafter annealed gradually from 800 K to target temperatures within 20 ns. All annealed simulation systems were equilibrated in an isothermal-isobaric ensemble for 80 ns of physical time maintained using a Nosé-Hoover thermostat and a Parrinello-Rahman barostat with time coupling constants of 0.4 and 0.2 ps, respectively, to control temperatures and pressure at 1 atm. Atomistic simulations were further performed in a canonical ensemble for 40 ns, and simulation trajectories were recorded at an interval of 100 fs for further analysis of microstructures and dynamical quantities of ion groups in IL matrices.

Additional atomistic simulations were performed on three triazolium ILs consisting of $[BF_4]$ anions and 1-alkyl-3-ethyl-1,2,3-triazolium ($[C_2C_n$TM-2-Triz$]$), 1-alkyl-3-ethyl-1,3,4-triazolium ($[C_2C_n$TM-4-Triz$]$), and 1-alkyl-3-ethyl-1,3,5-triazolium ($[C_2C_n$TM-5-Triz$]$) cations (n=2, 4 and 8) to explore the transferability of the constructed CG model and the derived interaction parameters in describing static and structural properties of triazolium ILs at relevant thermodynamic conditions. The atomistic FF parameters for triazolium cations were taken from our previous work [3], and the simulation parameters and procedures are the same with that for atomistic simulations of imidazolium ILs at varied thermodynamic states.

II. CG MD simulations of $[C_2C_nIM][BF_4]$ ILs

Interaction parameters for CG model. The constructed CG model for $[C_2C_nIM][BF_4]$ ILs are shown in Fig. S1. The blue and magenta spheres are labelled as "IM" and "BF" representing positively charged imidazolium ring and negatively charged $[BF_4]$ anion with partial charges of $+1.0e$ and $-1.0e$, respectively. The cyan beads representing ethyl and ethylene units in atomistic models are neutral spheres with the same set of force field parameters. Herein the head and tail ethyl units are labelled as "CH" and "CT", respectively, and the others are termed as "CE" for convenience of discussion. The CH and CT beads are specifically highlighted with different colors in relevant subsections to address their distributions in representative modelling systems.

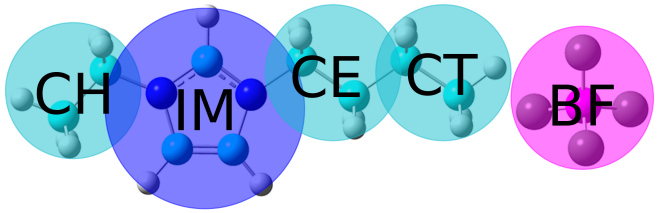

FIG. S1: Coarse-graining scheme for $[C_2C_4IM][BF_4]$ IL.

The bonded and non-bonded interaction potentials between CG beads are described by the AMBER FF format as shown in Eq. 1. The sizes of these CG beads are determined from their corresponding atomistic details and are listed in Table S1. The force field parameters for CG beads were first taken from previous work [5–8] and thereafter calibrated to reproduce microstructures and distribution functions of bond lengths, angles and dihedrals derived from atomistic references simulations, and are provided in Table S1.

CG MD simulation methodology. CG MD simulations of all model IL systems were performed using GROMACS package with similar simulation parameters unless explicitly addressed here. The equations of motion were integrated using a classical velocity Verlet leap-frog integration algorithm with a time step of 2.0 fs to accelerate CG MD simulations of IL systems at extended spatiotemporal scales with a modest computational cost. A cutoff distance of 1.6 nm was set for short range vdW interactions and real-space electrostatic interactions between atom-centered point charges. The Particle-Mesh Ewald summation method with an interpolation order of 5 and a Fourier grid spacing of 0.2 nm was employed

to handle long range electrostatic interactions in reciprocal space calculations. All model IL systems were first energetically minimized using a steepest descent algorithm, and thereafter annealed gradually from 1000 K to target temperatures within 20 ns and thereafter equilibrated in an isothermal-isobaric ensemble for 20 ns of physical time maintained using Nosé-Hoover thermostat and Parrinello-Rahman barostat with time coupling constants of 0.4 and 0.2 ps, respectively, to control temperatures and pressure at 1 atm. All CG MD simulations were sampled in a canonical ensemble for 100 ns, and simulation trajectories were recorded at an interval of 100 fs for further structural and dynamical analysis. In addition, this set of simulation parameters, unless explicitly stated, was adopted to explore thermotropic phase behaviors of monomeric ILs and to study ion association structures and ion transport quantities in polymeric ILs with different architectures.

TABLE S1: Force field parameters for the CG model for $[C_2C_nIM][BF_4]$ ILs.

Atom type	Mass (g/mol)	σ_{ii}(Å)	ϵ_{ii}(kJ/mol)	Charge q_i (e)
CH	29.07	4.120	1.2400	0.0
IM	67.07	4.380	2.5600	+1.0e
CE	28.06	4.120	1.2400	0.0
CT	29.07	4.120	1.2400	0.0
BF	86.81	4.510	3.2400	-1.0e

Bonds	r_0(Å)	K_r(kJ/mol Å^2))
CH-CH	2.500	300.0
CH-IM	3.025	500.0
IM-CE(CT)	3.025	500.0
CE-CE(CT)	2.500	300.0

Angles	θ_0 (deg)	K_θ(kJ/mol rad^2)
CH-IM-CE(CT)	140.0	100.0
IM-CE-CE(CT)	180.0	20.0
CE-CE-CE(CT)	180.0	20.0
CH-CH-IM	90.0	20.0
CH-CH-CH	180.0	20.0

Dihedrals	γ(deg)	K_ϕ(kJ/mol)	n
CH-IM-CE-CE(CT)	180.0	0.900	1
CH-IM-CE-CE(CT)	0.0	0.500	2
CH-IM-CE-CE(CT)	0.0	0.200	3
CH-IM-CE-CE(CT)	0.0	-0.200	4
IM(CE)-CE-CE-CE(CT)	180.0	0.900	1
IM(CE)-CE-CE-CE(CT)	0.0	0.300	2
IM(CE)-CE-CE-CE(CT)	0.0	0.200	3
IM-CH-CH-IM(CH)	0.0	0.100	1
CH-CH-IM-CE(CT)	90.0	0.100	1
CH-CH-CH-CH	180.0	0.100	1

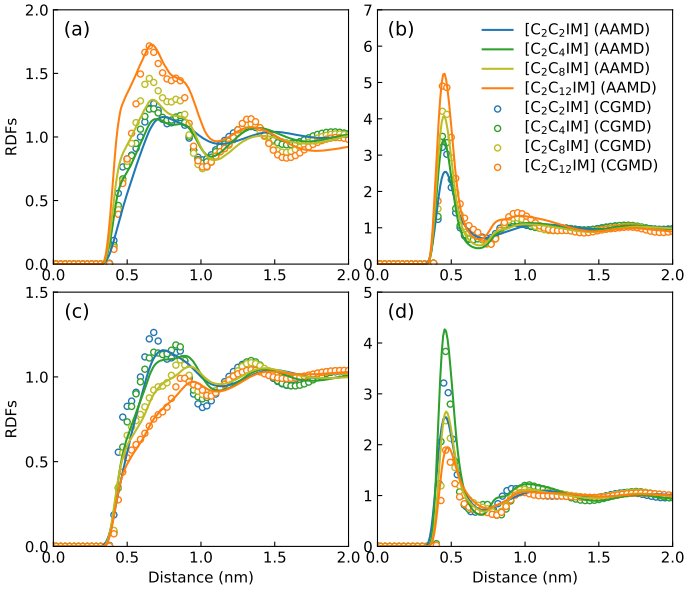

FIG. S2: Representative RDFs of (a) CH-IM, (b) CH-BF, (c) IM-CE(CT), and (d) BF-CE(CT) pairs for $[C_2C_nIM][BF_4]$ ILs obtained from AA and CG MD simulations performed at 400 K.

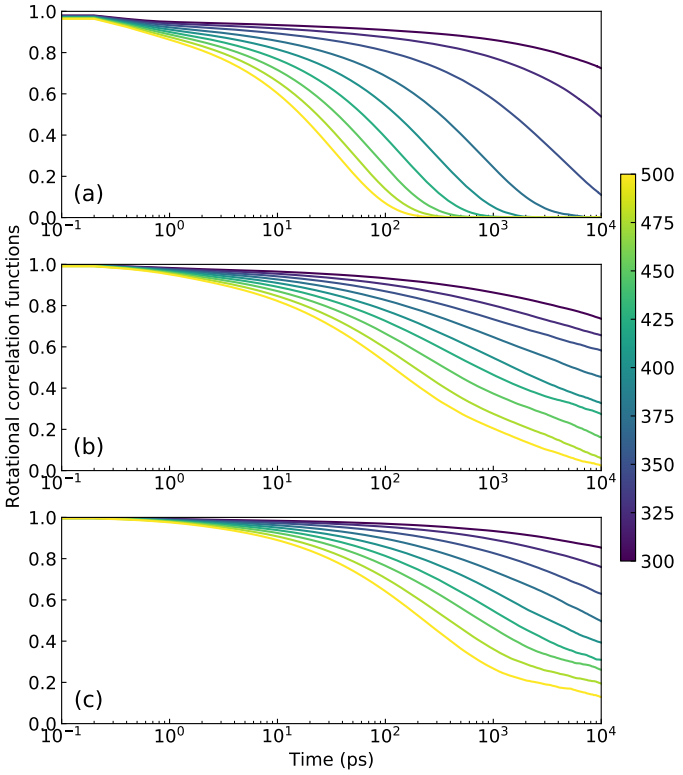

FIG. S3: Rotational correlation functions of CG (a) $[C_2C_4IM]$, (b) $[C_2C_{12}IM]$, and (c) $[C_2C_{20}IM]$ cations at varied temperatures.

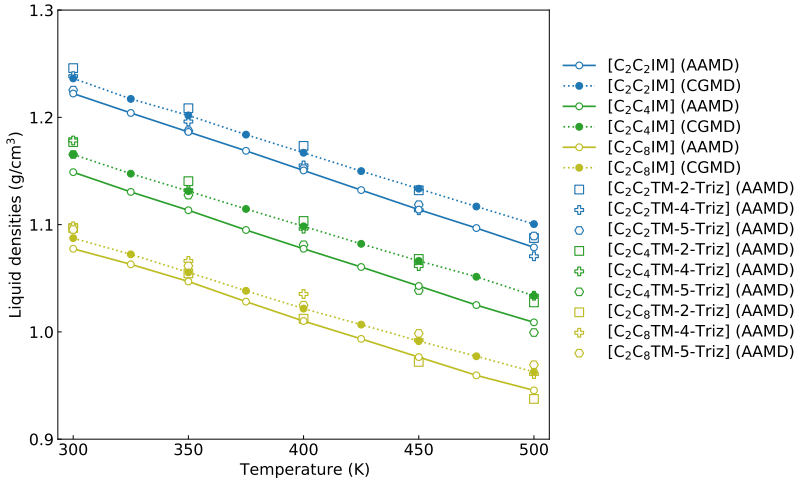

FIG. S4: Temperature-dependent liquid densities of [C_2C_nIM][BF_4] ILs obtained from AA and CG MD simulations are compared with computational data for triazolium ILs having varied alkyl chains obtained from atomistic simulations.

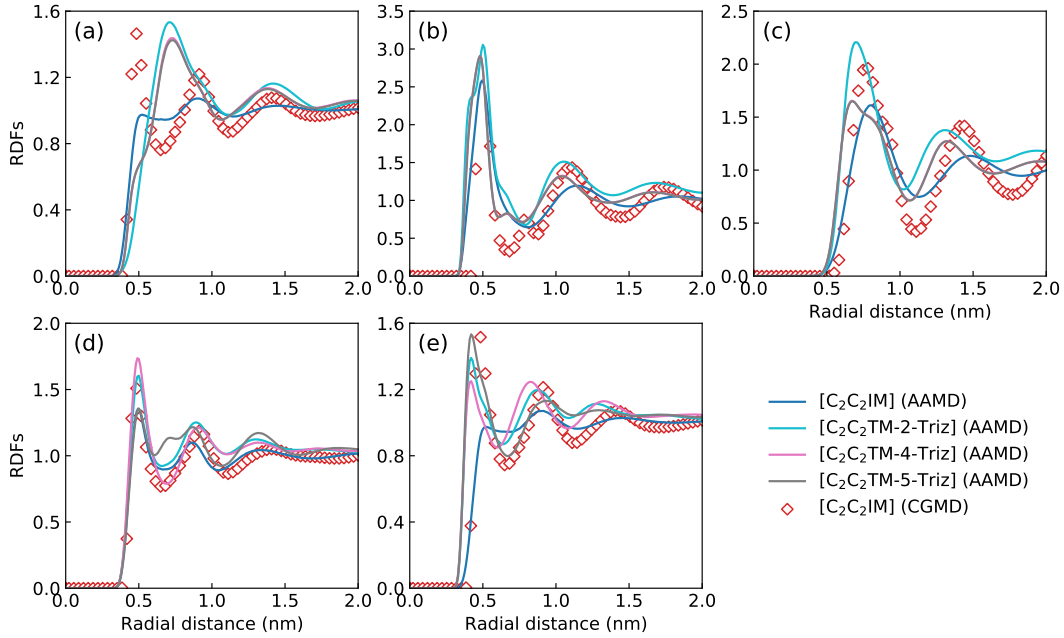

FIG. S5: Representative RDFs of (a) IM-IM, (b) IM-BF, (c) BF-BF, (d) CH-CH, and (e) CT-CT pairs for [C_2C_2IM][BF_4] ILs obtained from reference AA and CG MD simulations are compared with those determined from atomistic modelling of [C_2C_2TM-2-Triz][BF_4], [C_2C_2TM-4-Triz][BF_4], and [C_2C_2TM-5-Triz][BF_4] ILs at 400 K.

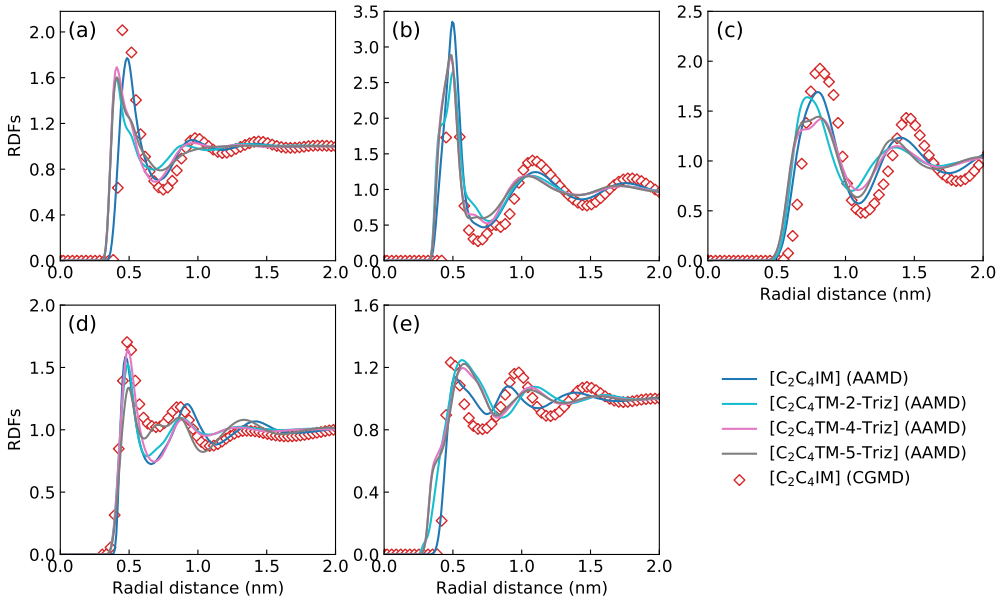

FIG. S6: Representative RDFs of (a) IM-IM, (b) IM-BF, (c) BF-BF, (d) CH-CH, and (e) CE(CT)-CE(CT) pairs for $[C_2C_4IM][BF_4]$ ILs obtained from reference AA and CG MD simulations are compared with those determined from atomistic modelling of $[C_2C_4TM\text{-}2\text{-}Triz][BF_4]$, $[C_2C_4TM\text{-}4\text{-}Triz][BF_4]$, and $[C_2C_4TM\text{-}5\text{-}Triz][BF_4]$ ILs at 400 K.

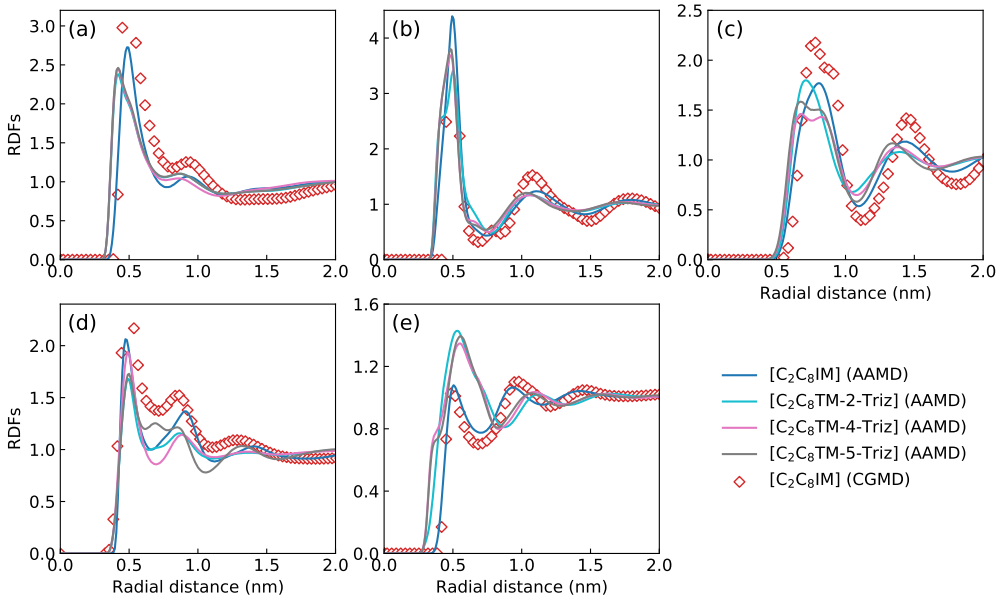

FIG. S7: Representative RDFs of (a) IM-IM, (b) IM-BF, (c) BF-BF, (d) CH-CH, and (e) CE(CT)-CE(CT) pairs for $[C_2C_8IM][BF_4]$ ILs obtained from reference AA and CG MD simulations are compared with those determined from atomistic modelling of $[C_2C_8TM\text{-}2\text{-}Triz][BF_4]$, $[C_2C_8TM\text{-}4\text{-}Triz][BF_4]$, and $[C_2C_8TM\text{-}5\text{-}Triz][BF_4]$ ILs at 400 K.

III. CG MD simulations of ILC phases

For CG MD simulations of thermotropic phase behaviors of ILs with varied cation alkyl chains, the $[C_2C_2IM][BF_4]$, $[C_2C_4IM][BF_4]$, $[C_2C_8IM][BF_4]$, $[C_2C_{12}IM][BF_4]$, $[C_2C_{16}IM][BF_4]$, $[C_2C_{20}IM][BF_4]$ modelling systems contain 13750, 11250, 8750, 7500, 6250, and 5000 ion pairs, respectively. The initial configurations of $[C_2C_nIM][BF_4]$ ion pairs were built in a lamellar form, resembling a smectic A phase with each layer in xy plane composed of 25*25 ion pairs and the xy plane area of (10*10) nm^2. Therefore, the above mentioned IL modelling systems have 22, 18, 14, 12, 10, and 8 IL layers, respectively, leading to the box lengths of these modelling systems along z-axis being $\sim$ 26.0 nm.

In all CG MD simulations, a semi-isotropic Parrinello-Rahman barostat was adopted to control pressure at xy plane and at z-axis at 1 atm. These modelling systems were performed in a sequential heating cascade from 50 to 500 K with a temperature interval of 50 K. The computational data from each temperature step were generated starting from the final configuration of the previous (lower) temperature, to allow for a more gradual thermal relaxation. Each CG MD simulation was allowed to equilibrate for 10 ns, during the initial temperature ramp, and thereafter to sample IL configurations in another 10 ns for structural and dynamical analysis.

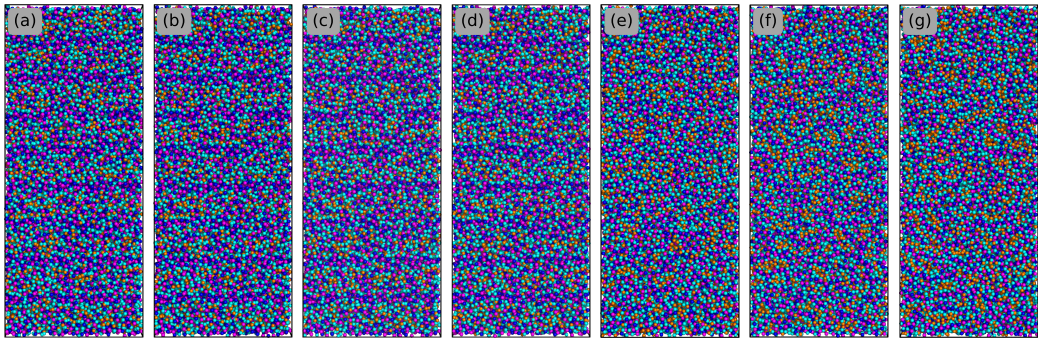

FIG. S8: Representative configurations of $[C_2C_4IM][BF_4]$ ILs in equilibrated simulation systems obtained from a sequential heating cascade. The tail CT beads in CG $[C_2C_4IM]$ cations are represented by orange spheres to highlight their spatial distributions in modelling systems. (a)-(g) correspond to $[C_2C_4IM][BF_4]$ ILs at 100, 200, 300, 350, 400, 450, and 500 K, respectively.

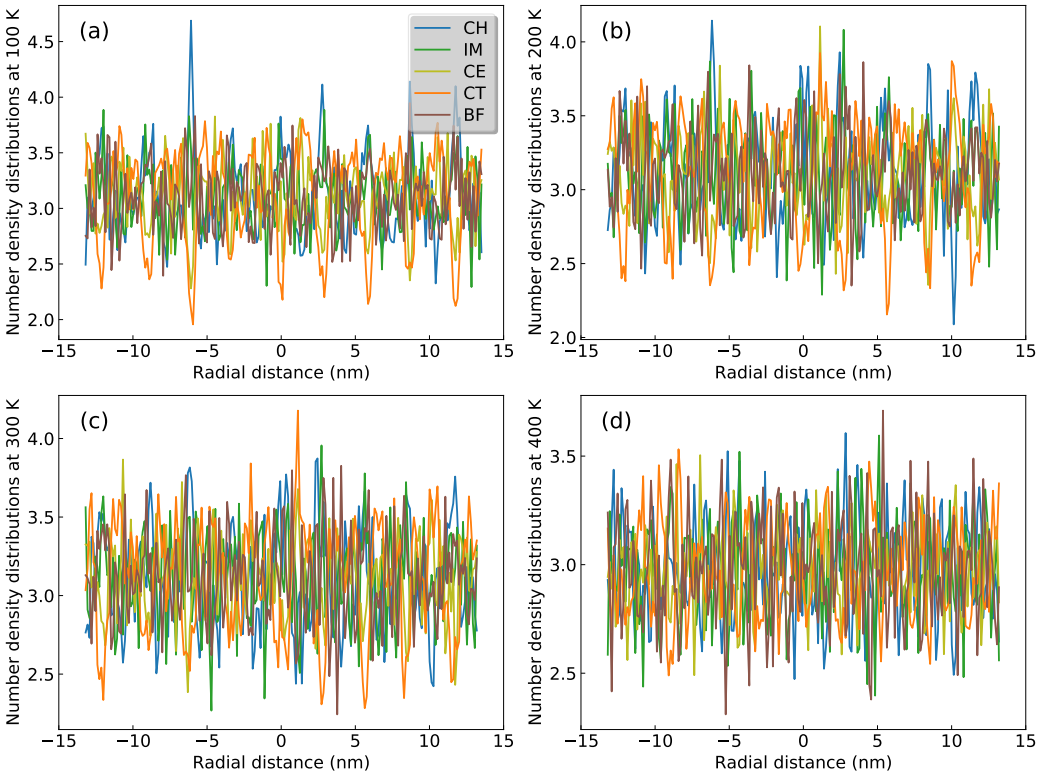

FIG. S9: Number density profiles of CG beads in $[C_2C_4IM][BF_4]$ ILs along z-axis at (a) 100 K, (b) 200 K, (c) 300 K, and (d) 400 K.

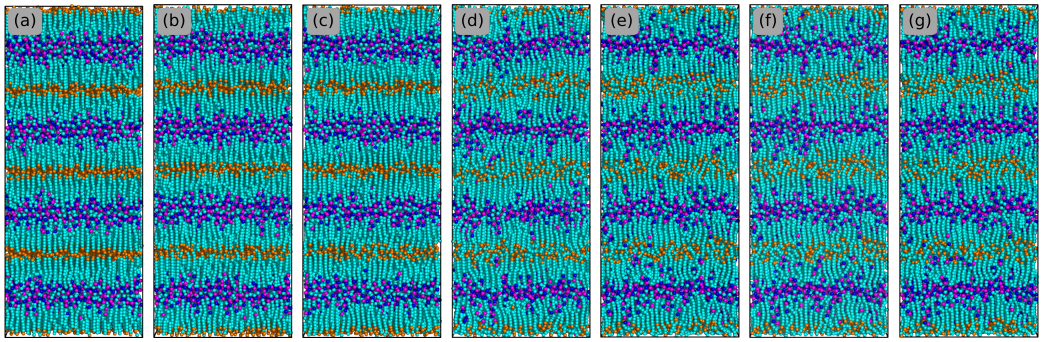

FIG. S10: Representative configurations of $[C_2C_{20}IM][BF_4]$ ILs in equilibrated simulation systems obtained from a sequential heating cascade. The tail CT beads in CG $[C_2C_{20}IM]$ cations are represented by orange spheres to highlight their spatial distributions in modelling systems and the formation of lamellae structures at low temperatures. (a)-(g) correspond to $[C_2C_{20}IM][BF_4]$ ILs at 100, 200, 300, 350, 400, 450, and 500 K, respectively.

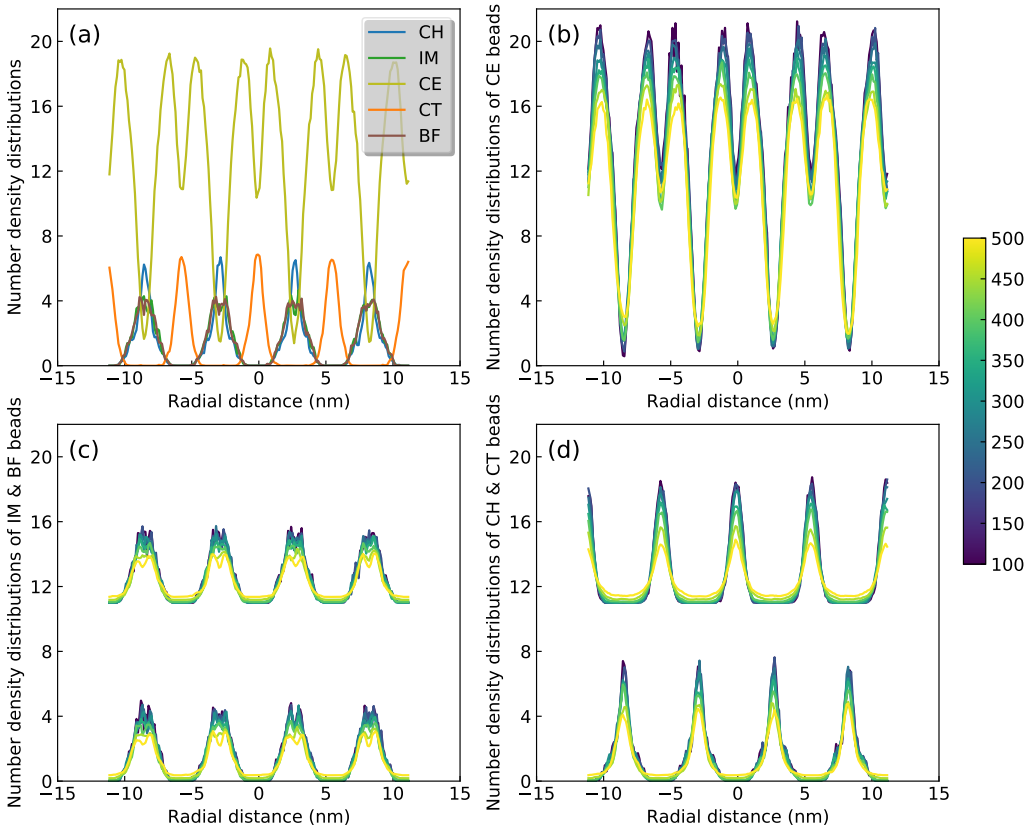

FIG. S11: Number density distributions of (a) CG beads in $[C_2C_{20}IM][BF_4]$ ILs along z-axis at 300 K, and of (b) CE, (c) IM and BF, and (d) CH and CT beads at different temperatures. The density profiles for BF and CT beads are vertically shifted by eleven units for clarity.

IV. CG MD simulations of backbone and pendant PILs

Backbone and pendant polymerized [C_2C_8IM] cations are constructed with PIL backbone lengths ranging from 6 to 60 to explore the effects of PIL architectures and PIL molecular weights on ion mobilities and the mechanism underlying ion association dynamics, ion hopping, and anion-PIL cation monomer coordinations. A series of BPIL chains consisting of 1, 2, 3, 4, 5, 6, 8, and 10 [C_2C_8IM] cation monomers with a head-to-tail polymerization manner is constructed with BPIL backbones consisting of 6, 12, 18, 24, 30, 36, 48, and 60 CG beads (each [C_2C_8IM] cation consists of 6 CG beads). Likewise, multiple PPIL chains are constructed with PPIL backbones containing 6, 12, 18, 24, 30, 36, 48, and 60 CH beads with a head-to-head polymerization form. Each modelling system contains 3600 [C_2C_8IM][BF_4] ion pairs with different number of BPIL and PPIL chains. The CG MD simulations parameters of BPIL and PPIL simulation systems are similar to that described in Section .

[1] Z. Liu, S. Huang, and W. Wang, J. Phys. Chem. B **108**, 12978 (2004).

[2] Y.-L. Wang, F. U. Shah, S. Glavatskih, O. N. Antzutkin, and A. Laaksonen, J. Phys. Chem. B **118**, 8711 (2014).

[3] Y.-L. Wang, J. Phys. Chem. B **124**, 7452 (2020).

[4] M. J. Abraham, T. Murtola, R. Schulz, S. Pall, J. C. Smith, B. Hess, and E. Lindahl, SoftwareX **1**, 19 (2015).

[5] D. Roy, N. Patel, S. Conte, and M. Maroncelli, J. Phys. Chem. B **114**, 8410 (2010).

[6] C. Merlet, M. Salanne, and B. Rotenberg, J. Phys. Chem. C **116**, 7687 (2012).

[7] Y.-L. Wang, Y.-L. Zhu, Z.-Y. Lu, and A. Laaksonen, Soft Matter **14**, 4252 (2018).

[8] O. Y. Fajardo, S. Di Lecce, and F. Bresme, Phys. Chem. Chem. Phys. **22**, 1682 (2020).